JOURNAL OF MATERIALS SCIENCE 32 (1997) 2969–2975

Characterization of SiC/C (B)/SiC microcomposites by transmission electron microscopy

S. JACQUES, A. GUETTE, F. LANGLAIS, X. BOURRAT
Laboratoire des Composites Thermostructuraux, Unité Mixte de Recherche, Université CNRS-Société-UB1 47, Bordeaux I, 3 allée de la Boëtie, 33600 Pessac, France

Uniform or composition-graded C(B) (i.e., boron-containing carbon) interphases in SiC/SiC model microcomposites were characterized by transmission electron microscopy after tensile tests and thermal ageing in air. A specific method was developed to prepare thin longitudinal sections of the tested specimens. Deflection of matrix cracks occurs within the uniform C(B) interphase, as long as its anisotropy remains high enough (i.e., when the boron content is not too high). It takes place close to the most anisotropic layer (i.e. that containing 8 at % of boron) in composition-graded interphases. In both cases, the crack deflection path does not reach the fibre, a feature which is consistent with the good mechanical properties. After ageing in air under tensile loading beyond the proportional limit (600 °C; $\sigma = 800$ MPa), the composition-graded interphase (made of five sublayers in which the boron content increases from 0 at % near the fibre to 33 at % near the matrix) was observed to act as a glass-forming protection, the pyrocarbon sublayer (at the fibre surface) remaining unoxidized.

1. Introduction

The thermomechanical behaviour of ceramic matrix composites can be controlled by depositing on the fibre a thin film, referred to as the "interphase", prior to the infiltration of the matrix. An understanding of the micromechanics involved during mechanical loading or under oxidizing conditions can be achieved using transmission electron microscopy (TEM) [1, 2] (i.e., by observation of the crack propagation modes).

In the present study, a single-filament test specimen was used (microcomposite). A single fibre 50 mm long was successively coated by two layers: first a thin film of interphase and then a thicker layer of matrix. This kind of specimen, which can be easily prepared by chemical vapour deposition (CVD), has been recently used to study the mechanical properties [3, 4] or to develop and characterize new kinds of interphase [5, 6]. A method for making thin longitudinal sections of microcomposites was developed and successfully applied to SiC/SiC microcomposites.

The aim of the present contribution is to report TEM characterization which has been performed on uniform or composition-graded C(B) interphases (CGIs) developed in a previous paper [6] in order firstly to confirm the nature of the successive layers with different compositions constituting the CGIs, secondly to link their mechanical characteristics to the crack deflection paths and thirdly to observe their evolution when submitted to oxidation conditions.

2. Experimental procedure

In the direct ion thinning technique of a longitudinal section of a microcomposite (or a fibre), the thinning occurs circumferentially, which sharpens the fibre. So, the thin area is obtained close to the fibre core and not near its external surface or the interphase. Berger and Bunsell [7] have proposed, for simple fibres, to align and set them in contact with each other on a copper ring. Thus, each fibre surface is protected from the Ar^+ beams by adjacent fibres and thus the chance to obtain a thin section of the fibre surface is increased (Fig. 1). Unfortunately, it was very difficult to use this method because of the space left between microcomposites, leading to a sharpening of the microcomposite tip. Thus, a simple and rapid method was developed in the case of specimen sparseness.

A few microcomposites (at least three) were laid parallel, not necessarily in contact with each other, on a silicon slab. Each microcomposite was at least 3 mm long. A drop of epoxy resin (Micro-Measurements-Vishay adhesive, M-Bond 610) was then carefully deposited, so that microcomposites are kept aligned on the slab as shown in Fig. 2a. The microcomposites and the resin were then covered with a second silicon slab. The whole sample submitted to a slight pressure was heated in a drying oven at 160 °C for 2 h (Fig. 2b). After curing, the two silicon slabs were removed, yielding a thin hard resin sheet which contained the microcomposites, with a total thickness of about 20 μm, i.e., the microcomposite diameter (Fig. 2c). Then, it was stuck on the TEM slot copper grid (1 mm wide and 2 mm long) (Fig. 2d). The sample prepared thus was then ion milled (dual ion mill 600 from Gatan) at room temperature. This method enabled us to fill in totally the spaces between two adjacent microcomposites with resin which protects the side surfaces from too rapid ion beam milling.

0022–2461

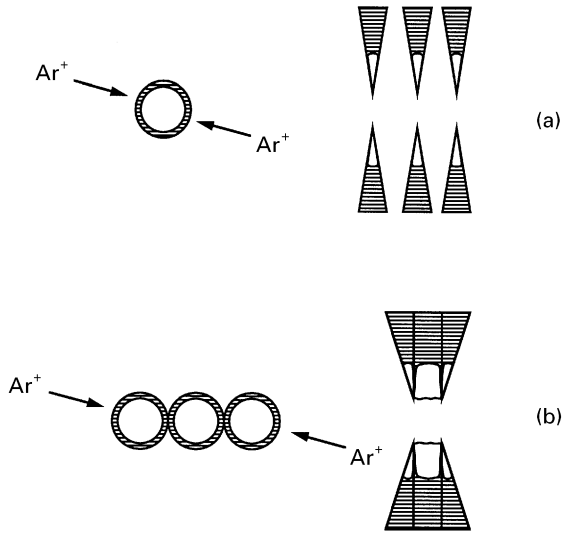

Figure 1 Ion thinning of fibres in longitudinal sections according to Berger and Bunsell [7]. (▤), fibre surface; (□), fibre core. (a) Isolated fibres are ion thinned circumferentially and the fibre surface is removed. (b) The surface of the fibre in the middle is protected from the ion beam by the adjacent fibres and is still present on the observable thin regions.

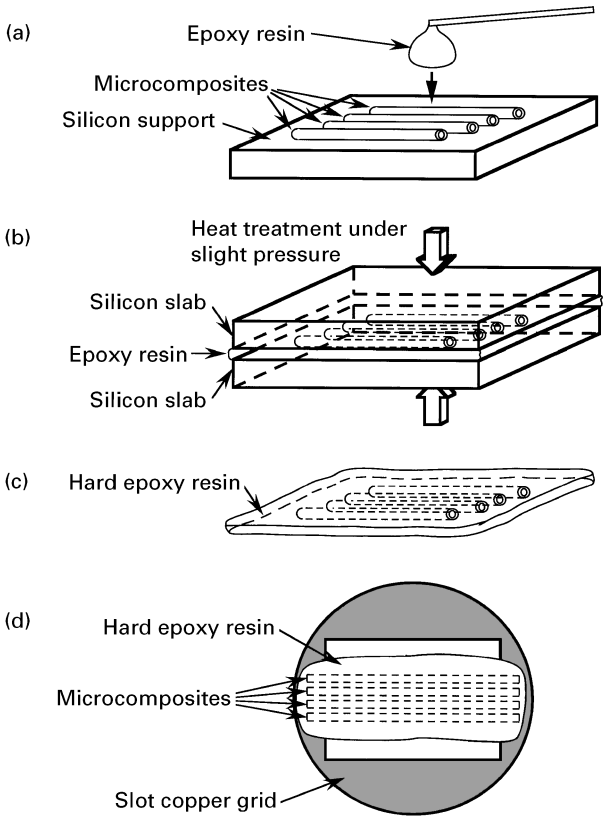

Figure 2 Method for making thin longitudinal sections of microcomposites.

This technique was applied to SiC/SiC microcomposites after tensile tests, performed at room temperature up to failure. These microcomposites were made of Nicalon single fibres (NL 200) 14 μm in diameter coated successively with firstly a boron-containing carbon C(B) interphase (0.4–0.5 μm thick) and secondly the SiC matrix (about 2.5 μm thick). They were prepared and tested as reported in [6]. The

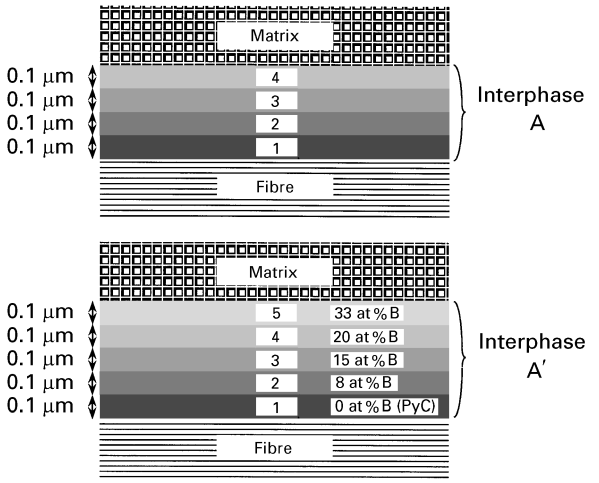

Figure 3 Schematic diagrams of the interphases A and A′.

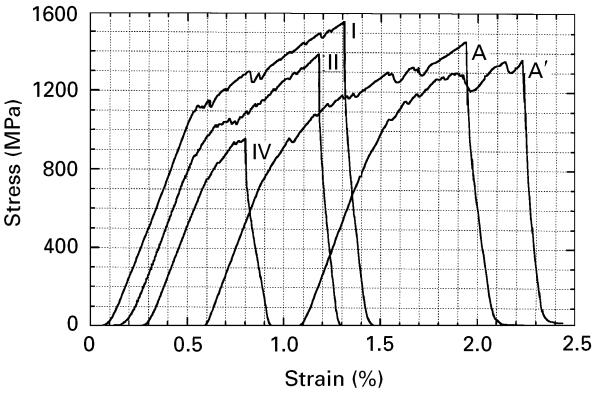

Figure 4 Typical tensile stress–strain curves at room temperature for SiC/SiC microcomposites with uniform interphases I, II and IV and CGIs A and A′ (curves are offset horizontally for clarity).

interphases were made of C(B) materials with different uniform boron contents (I, pyrocarbon (PyC); II, 8 at % B; IV, 20 at % B) or CGIs A and A′ as schematically shown in Fig. 3. In the A-type CGI, the interfacial sequence contained four sublayers in which the boron content increases by steps, between 0 at % B near the fibre to 20 at % B near the matrix. In the A′-type CGI, an extra sublayer with about 33 at % B was added near the matrix. These various microcomposites were tensile tested at room temperature and their typical behaviour is given in Fig. 4. Matrix crack deflections within interphases were observed by TEM (Philips CM 30 ST), according to the contrasted bright-field (BF) mode. The matrix cracks are not artiefacts due to thin-foil preparations, since such cracks have never been observed within microcomposites prepared in the same way which had not been tensile tested. Moreover, the resin selected for that preparation was usually observed within the matrix cracks, demonstrating that they pre-existed before the sampling.

Microcomposites with interphase A′ were also thinned and observed by TEM after thermal ageing in air at 600 °C under load (the applied stress was chosen at 800 MPa, i.e., slightly above the proportional limit), using a previously described procedure [6]. A parallel

electron-energy-loss spectrometer (Gatan) was used with an electron probe size of about 20 nm, for chemical elemental analyses of the oxidized interphase.

3. Results and discussion

3.1. Single-layered interphase

Fig. 5a and b present typical crack deflections observed in microcomposites with uniform interphases I and II, respectively, after tensile tests. In both cases, they occur within the interphase itself and not at the fibre surface. These results are consistent with the good mechanical properties observed for these microcomposites (average stress to failure, 1600 MPa and 1350 MPa for microcomposites I and II, respectively) [6]. This feature has been reported to correspond to a "cohesive" failure mode for actual two-dimensional SiC/PyC/SiC composites [1]. It is produced by a strong bonding of the interphase with the fibre. On line is the very low matrix crack spacing observed in that case (Fig. 5a, in which three matrix cracks observed in an area 10 μm long). These behaviours (i.e., cohesive failure mode and low crack spacing) are the micromechanical evidences of a matrix cracking-based toughening. This is an alternative interfacial behaviour to the debond–sliding mechanism, in which the interface first debonds ("adhesive" failure), and where the major contribution to toughness involves sliding of the fibres along the debonded interfaces [8].

Fig. 5c shows one of the very few cracks which could be observed in tested microcomposites with interphase IV. For this microcomposite, rather poor tensile characteristics were observed (average stress to failure, 985 MPa). It is assumed that the first matrix cracks that appear during the tensile test lead most of the time to failure, as shown in the stress–strain curve in Fig. 4. In Fig. 5c, the crack propagates across the whole interphase and is deflected directly at the fibre surface. Here the bulk of the interphase does not play the role of matrix crack deflector. It has been shown in a previous paper [9] that for such a boron concentration in PyC (20 at %) the texture is no longer laminar but has become isotropic.

3.2. Multilayered interphase

Fig. 6 shows an observation of the CGI A′ made up of five C(B) sublayers with different boron contents. The successive sublayers can be easily distinguished owing to the different contrasts resulting from their different textures [9]. After tensile tests, most of the microcomposites exhibited an extensive debonding at the layer 2–layer 3 interface. This debonding may be due to thermal residual stress after the CVD preparation at 950 °C. Layer 2, which is rather highly anisotropic, is assumed to exhibit distinct coefficients of thermal expansion (CTEs), α, depending on the direction: lower along the fibre axis than perpendicular to it (for graphite, $\alpha = 1 \times 10^{-6}\,°C^{-1}$ within graphite layers and $\alpha = 15 \times 10^{-6}\,°C^{-1}$ perpendicular to the graphite layers). Conversely, layer 3, which is more isotropic, may have different CTEs. As a consequence, radial and/or shear stresses may occur at that interface. These internal stresses are released when the matrix cracks. This relaxation allows matrix cracks to be deflected, as shown in Fig. 7. In that case, deflection occurs far from the fibre surface, before they reach layer 1 (PyC), which is favourable for a good oxidation resistance. With regard to the ultimate performance, it was seen that this interfacial behaviour resulted in high strength and strain to failure (average stress to failure, 1340 MPa) [6]. For interphase A (average stress to failure, 1490 MPa), we could observe a crack multideflection at different levels of the multilayer (Fig. 8). Thus, arrangement of the different layers can

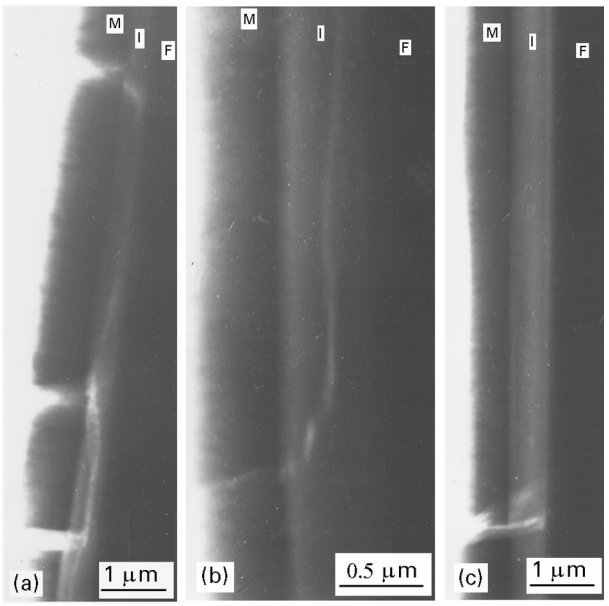

Figure 5 Bright-field images of matrix crack deflections in microcomposites with uniform C(B) interphases: (a) I (PyC); (b) II (8 at % B); (c) IV (20 at % B). M, matrix; I, interphase; F, fibre.

Figure 6 Bright-field image of matrix crack deflection (arrows) in compositional gradient interphase A′. F, fibre; M, matrix; the numbers relate to the five different sublayers involved in the interphase.

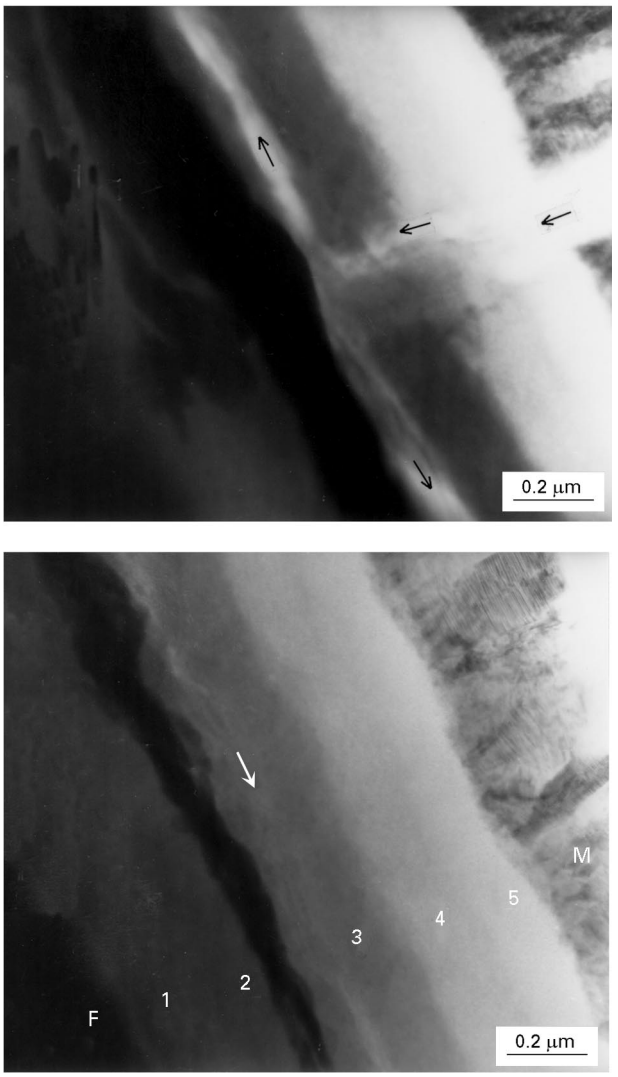

Figure 7 Bright-field images of matrix crack deflection in compositional gradient interphase A′. The dark areas in layer 2 reveal the presence of polycrystalline structures.

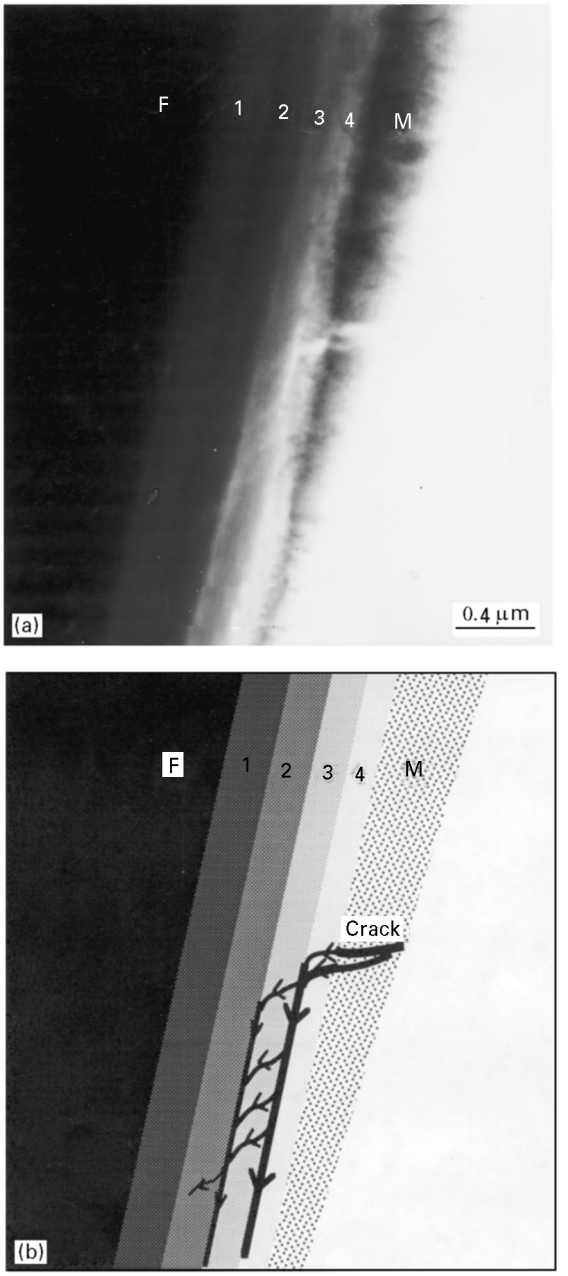

Figure 8 A matrix crack deflection in compositional gradient interphase A: (a) bright-field image; (b) schematic diagram.

control the crack deflection path within the interphase. This is very favourable, since multideflection is energy absorbing and thereafter participates in toughening as previously demonstrated [1].

3.3. Uncontrolled crystal growth

During TEM observations in BF mode of microcomposite thin longitudinal sections, dark areas appeared in interphase II (Fig. 9) or in layer 2 of the CGIs (Fig. 7). This particular phase is systematically present in the C(B) material containing about 8 at % B [9]. However, the content of this phase in the C(B) layer is rather low. The selected-area diffraction (SAD) pattern over an area containing this phase (Fig. 10) reveals clearly the existence of submicrometric polycrystalline structures. High-resolution TEM observations and parallel electron-energy-loss spectroscopy (PEELS) chemical analyses were not possible because of the difficult thinning of this heterogeneous material. Inter-reticular distances, d, calculated from the SAD pattern, and a tentative index linking in the face-centred cubic (f.c.c.) lattice (with a lattice parameter of 358 pm) are given in Table I. Fig. 11 shows a microdiffraction pattern (electron probe diameter, 10 nm) with a fourfold symmetry axis corresponding to the f.c.c. lattice. As the crystallites are very small, the pattern is not even in contrast owing to lattice deformations. Such a lattice does not correspond to any boron carbide usually deposited by CVD (B_4C, $B_{13}C_2$, $B_{50}C_2$, etc.) [10–12], nor to pure boron [12]. Fig. 12 gives a SAD pattern obtained with the incident electron beam along the [110] direction. Such a diagram could be related to a diamond structure with $\{111\}$ planar defects (twins), but also irregular stacking faults as shown by the occurrence of streaky spots in the [111] direction. This has already been reported by many workers for the small diamond crystal sizes obtained at high nucleation rate [13–16]. The presence of a diamond structure phase is unexpected because external excitations such as a high-temperature

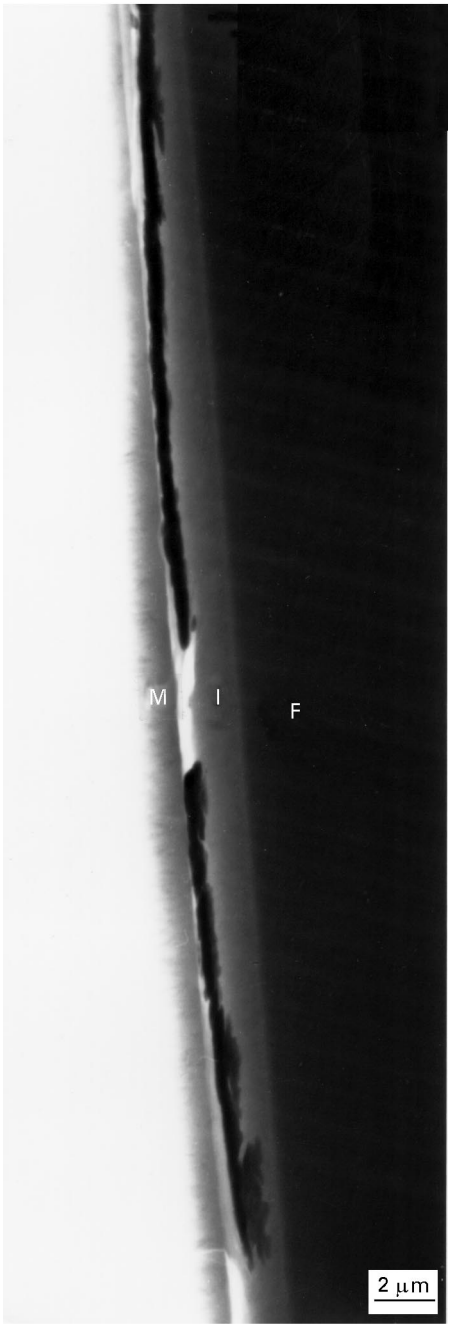

Figure 9 Bright-field image of a microcomposite with interphase II. The dark areas in the interphase correspond to the polycrystalline structures.

filament or plasma or flame were not present. Nevertheless, diamond formation could be explained by the presence of halogens and boron in the reactional H_2-rich mixture, in accordance with previous work [17, 18].

3.4. Ageing treatment in air

Observations of interphases A′ after ageing treatment in air reveal areas where the interphase remains entirely intact and others where it is partially oxidized as shown in Fig. 13. It has been difficult to correlate these observations with the presence of matrix cracks, because thin areas were not extended enough. In Fig. 13, layers 3, 4 and 5 have been replaced by an amorphous

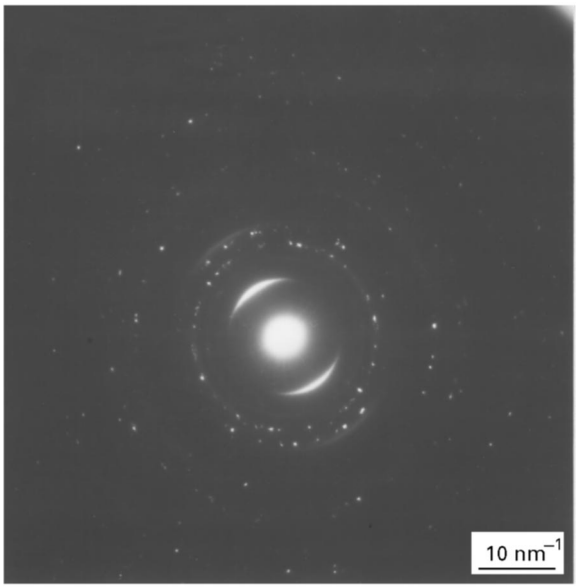

Figure 10 An electron SAD pattern from the polycrystalline phase evidenced in Figs 7 and 9.

TABLE I Miller indices and inter-reticular distances, *d*, calculated from the SAD patterns of the polycrystalline phase evidenced in Figs 7 and 9.

hkl	*d*(pm)
111	207
200	179
220	127
311	108
222	103
400	90
331	82
420	80
422	73

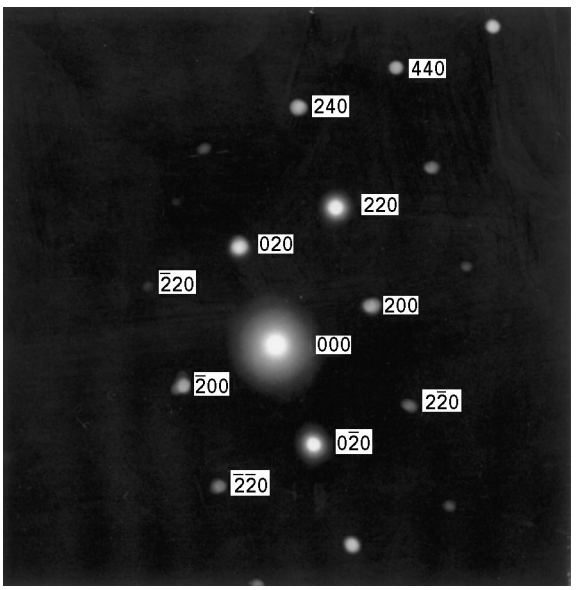

Figure 11 Microdiffraction pattern of a single crystal which belongs to one of the dark areas of interphase II evidenced in Fig. 9.

material (as shown by a diffuse SAD pattern) made of silica, as proved by PEELS analysis (Fig. 14). On location of layers 1 and 2, carbon is still present (Fig. 15). This preferential oxidation can be attributed

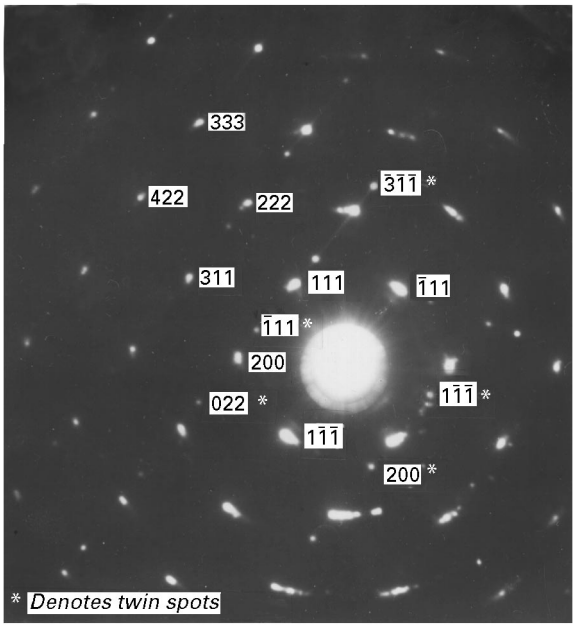

Figure 12 SAD pattern from a single crystal which belongs to one of the dark areas of interphase II evidenced in Fig. 9. This pattern is typical of a twinned and faulted diamond structure.

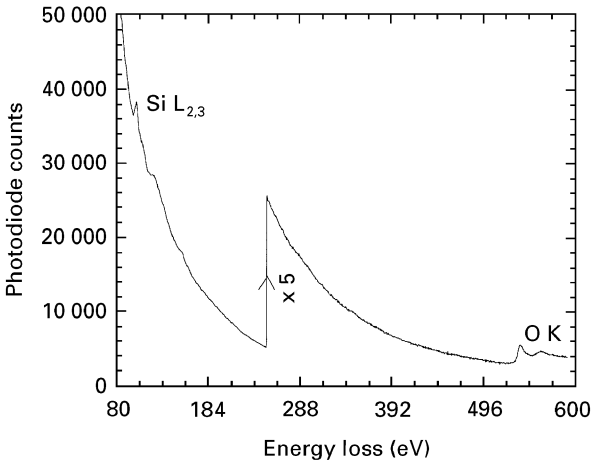

Figure 14 Electron-energy-loss spectra from the oxide occurring in layers 3–5.

to the path of matrix cracks. It is supposed that cracks allow oxygen diffusion to layers 3, 4 and 5 but not to layers 1 and 2 because the deflection occurs between layers 2 and 3. Furthermore, oxide has probably

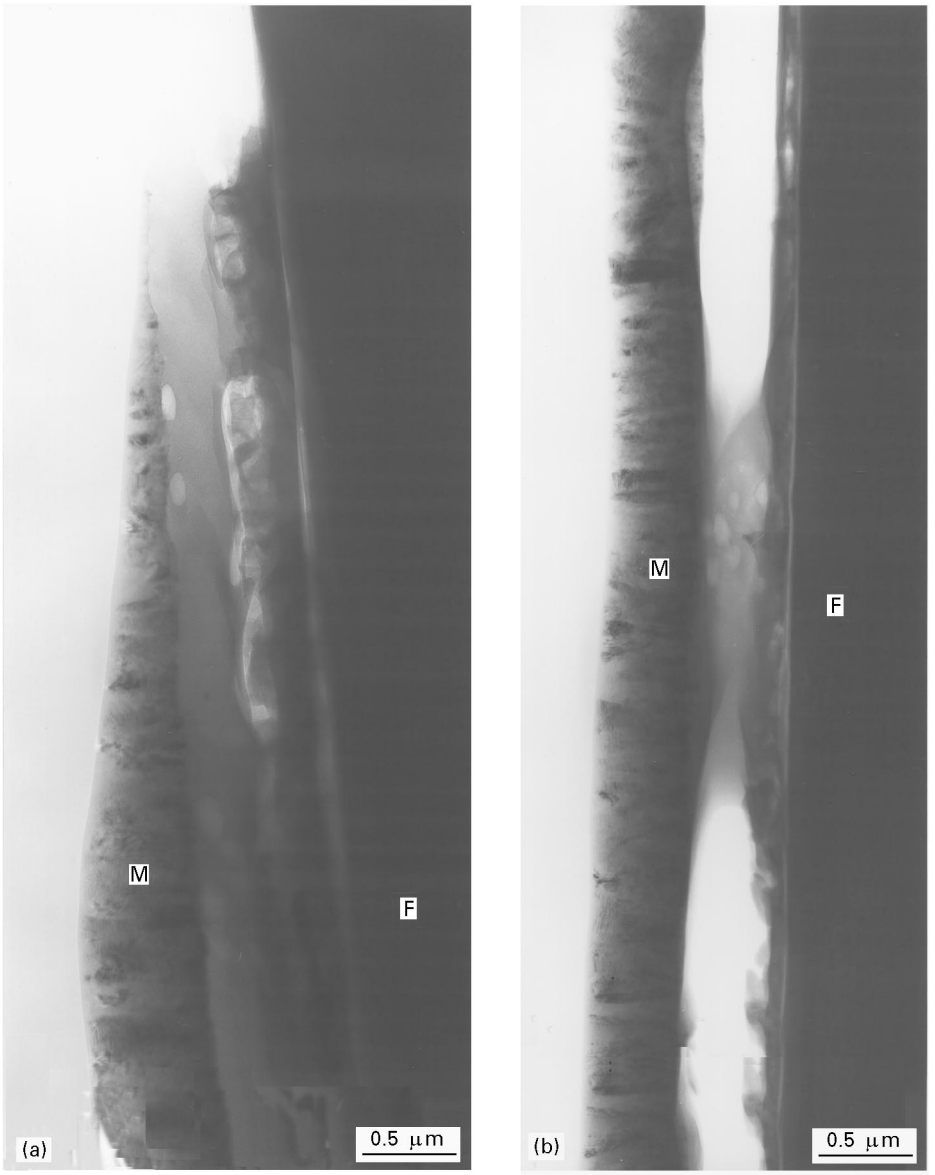

Figure 13 Bright-field images of a microcomposite with compositional gradient interphase A′ after ageing in air at 873 K under load.

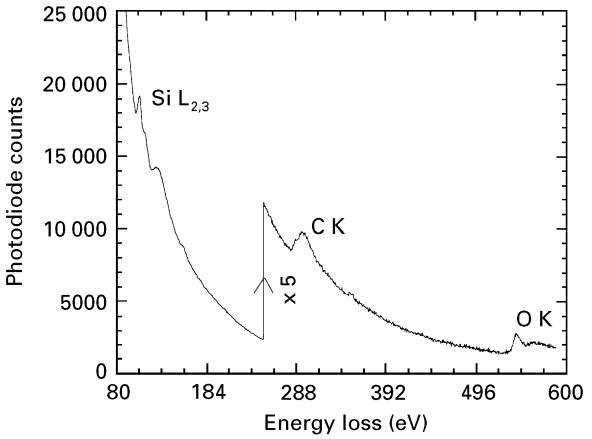

Figure 15 Electron-energy-loss spectra from the partially oxidized layer 2.

protected the first two layers from air; the glass forming-based protection of the three external sublayers appears efficient. The absence of boron in the oxide after ageing can be explained by the great sensitivity of B_2O_3 towards the moisture in the air, resulting in volatile boric acid formation [19–21]. This phenomenon might be enhanced (even at room temperature) for TEM samples because of their very low thickness.

4. Conclusion

A method for making thin longitudinal sections of microcomposites has been developed in order to characterize by TEM interphases in SiC/C(B)/SiC. The matrix crack deflection paths after tensile tests of these microcomposites were observed. It was confirmed that the good mechanical properties are due to a matrix crack deflection within the bulk of the interphase, before reaching the fibre.

This method allowed us to demonstrate by TEM the occurrence of a particular nano crystallized phase, which is embedded in a C(B) material with 8 at % B. On the basis of measurements from SAD patterns and their index linking, this phase was found to correspond to diamond structure with planar defects.

Finally, in the CGIs, an ageing in air results in the consumption of the boron-rich layers close to the matrix yielding, a silica-containing phase, which seems to protect the low boron content layers close to the fibre.

Acknowledgements

This work has been supported by CNRS and SEP through a grant to S. Jacques. The authors wish to thank M. Alrivie for her contribution to sampling techniques and R. Naslain for a fruitful discussion.

References

1. C. DROILLARD, J. LAMON and X. BOURRAT, *Mater. Res. Soc. Symp. Proc.* **365** (1995) 371.
2. N. FRETY, R. MOLINS and M. BOUSSUGE, *J. Mater. Sci.* **27** (1992) 5084.
3. J. LAMON, C. RECHINIAC, N. LISSART and P CORNE, in "Proceedings of the fifth European Conference on Composite Materials", Bordeaux, 7–10 April 1992, edited by A. R. Bunsell, J. F. Jamet and A. Massiah (EACM-CEC, Paris, 1992) p. 895.
4. J. LAMON, F. REBILLAT and A. G. EVANS, *J. Amer. Ceram. Soc.* **78** (1995) 401.
5. S. JACQUES, A. GUETTE, F. LANGLAIS, R. NASLAIN and S. GOUJARD, in "Proceedings of the second International Conference on High-Temperature Ceramic-Matrix Composites, Santa Barbara, CA, 21–24 August 1995, Ceramic Transactions, Vol. 57, edited by A. G. Evans and R. Naslain (American Ceramic Society, Columbus, OH, 1995) p. 381.
6. S. JACQUES, A. GUETTE, F. LANGLAIS and R. NASLAIN, *J. Mater. Sci.* (1997) submitted.
7. M. H. BERGER and A. R. BUNSELL, *J. Mater. Sci. Lett.* **12** (1993) 825.
8. A. G. EVANS, *J. Amer. Ceram. Soc.* **73** (1990) 187.
9. S. JACQUES, A. GUETTE, X. BOURRAT, F. LANGLAIS, R. NASLAIN, C. GUIMON and C. LABRUGÈRE, *Carbon* **34** (1996) 1135.
10. K. PLOOG, *J. Cryst. Growth* **24–25** (1974) 197.
11. L. VANDENBULKE and G. VUILLARD, *J. Less-Common Metals* **82** (1981) 49.
12. "Powder diffraction file" (American Society for Testing and Materials, Philadelphia, PA, 1987) file no. 11-0617 and 12-0377.
13. G-H. M. MA, Y. H. LEE and J. T. GLASS, *J. Mater. Res.* **5** (1990) 2367.
14. K. SUZUKI, M. ICHIHARA, S. TAKEUCHI, N. OHTAKE, M. YOSHIKAWA, K. HIRABAYASHI and N. KURIHARA, *Phil. Mag. A* **65** (1992) 657.
15. W. ZHU, A. R. BADZIAN and R. MESSIER, *J. Mater. Res.* **4** (1989) 659.
16. R. F. DAVIS (ed.), "Diamond films and coatings" (Noyes Publications, Park Ridge, NJ, 1993) p. 303.
17. K. E. SPEAR and J. P. DISMUKES (eds), "Synthetic diamond: emerging CVD science and technology". Electrochemical Society Series (Wiley–Interscience, New York, 1994) p. 264.
18. D. E. PATTERSON, C. J. CHU, B. J. BAI, Z. L. XIAO, N. J. KOMPLIN, R. H. HAUGE and J. L. MARGRAVE, *Electrochem. Soc. Proc.* **8** (1991) 3.
19. L. M. LITZ and R. A. MERCURI, *J. Electrochem. Soc.* **110** (1963) 921.
20. D. W. McKEE, *Carbon* **24** (1986) 737.
21. K. KOBAYASHI, K. MAEDA, H. SANO and Y. UCHIYAMA, *ibid.* **33** (1995) 397.

Received 5 March
and accepted 19 December 1996